The Astrophysical Journal, 838:4 (8pp), 2017 March 20 https://doi.org/10.3847/1538-4357/aa6337

Lyα and UV Sizes of Green Pea Galaxies

Huan Yang[1,2], Sangeeta Malhotra[2], James E. Rhoads[2], Claus Leitherer[3], Aida Wofford[4], Tianxing Jiang[2], and Junxian Wang[1]
[1] CAS Key Laboratory for Research in Galaxies and Cosmology, Department of Astronomy, University of Science and Technology of China, China; huan.y@asu.edu
[2] Arizona State University, School of Earth and Space Exploration, USA
[3] Space Telescope Science Institute, 3700 San Martin Dr, Baltimore, MD 21218, USA
[4] National Autonomous University of Mexico, Institute of Astronomy, Mexico
Received 2016 October 17; revised 2017 February 23; accepted 2017 February 24; published 2017 March 17

Abstract

Green Peas are nearby analogs of high-redshift Lyα-emitting galaxies (LAEs). To probe their Lyα escape, we study the spatial profiles of Lyα and UV continuum emission of 24 Green Pea galaxies using the Cosmic Origins Spectrograph (COS) on the *Hubble Space Telescope*. We extract the spatial profiles of Lyα emission from their 2D COS spectra, and of the UV continuum from both 2D spectra and NUV images. The Lyα emission shows more extended spatial profiles than the UV continuum, in most Green Peas. The deconvolved full width at half maximum of the Lyα spatial profile is about 2–4 times that of the UV continuum, in most cases. Because Green Peas are analogs of high z LAEs, our results suggest that most high-z LAEs probably have larger Lyα sizes than UV sizes. We also compare the spatial profiles of Lyα photons at blueshifted and redshifted velocities in eight Green Peas with sufficient data quality, and find that the blue wing of the Lyα line has a larger spatial extent than the red wing in four Green Peas with comparatively weak blue Lyα line wings. We show that Green Peas and MUSE $z = 3$–6 LAEs have similar Lyα and UV continuum sizes, which probably suggests that starbursts in both low-z and high-z LAEs drive similar gas outflows illuminated by Lyα light. Five Lyman continuum (LyC) leakers in this sample have similar Lyα to UV continuum size ratios ($\sim$1.4–4.3) to the other Green Peas, indicating that their LyC emissions escape through ionized holes in the interstellar medium.

Key words: galaxies: dwarf – galaxies: high-redshift – galaxies: starburst – line: formation – radiative transfer – ultraviolet: ISM

1. Introduction

The Lyα emission line is a key tool in discovering and studying high-redshift galaxies (e.g., Dey et al. 1998; Hu et al. 1998; Rhoads et al. 2000; Ouchi et al. 2003; Matthee et al. 2014; Zheng et al. 2016). At $z > 6$, the Lyα luminosity, Lyα equivalent width (EW), and spatial clustering of Lyα emitting galaxies (LAEs) are important probes of the reionization of universe (e.g., Malhotra & Rhoads 2004; Kashikawa et al. 2011; Treu et al. 2012; Pentericci et al. 2014; Tilvi et al. 2014). To understand LAEs and reionization requires us to understand how Lyα escape from galaxies.

Because Lyα is a resonant line, the Lyα escape depends on the amount of dust, the H I gas column density ($N_{\rm H\,I}$), the velocity distribution of H I gas, and the geometric distribution of H I gas and dust (e.g., Neufeld 1990; Charlot & Fall 1993; Dijkstra et al. 2006; Verhamme et al. 2006). One important indicator of Lyα escape processes is the Lyα spatial distribution. The Lyα emission would be confined to H II regions and have similar size to the UV continuum emission, if most Lyα photons escape from ionized holes in the interstellar medium (ISM). However, if most Lyα photons diffuse out of a galaxy through numerous resonant scatterings, the Lyα emission would be more extended than the UV continuum (e.g., Östlin et al. 2009; Zheng et al. 2010; Hayes et al. 2014).

Prior *Hubble Space Telescope* (*HST*) studies of Lyα morphology in low-redshift starburst galaxies usually show diffuse Lyα emission in the outer part of galaxy, and sometimes Lyα absorption in the center of galaxy (Kunth et al. 2003; Mas-Hesse et al. 2003; Hayes et al. 2005, 2014; Östlin et al. 2009). But most of those low-redshift starbursts have much lower Lyα EW (EW < 20 Å) and Lyα escape fraction ($f_{\rm esc}^{\rm Ly\alpha}$) than high-$z$ LAEs. Because Lyα photons escape more easily and probably have fewer scatterings in high-z LAEs, it is reasonable to suppose that LAEs with high Lyα EW may have compact Lyα sizes. Due to the faintness of high-z LAEs, there are only two studies of Lyα size with high-resolution *HST* narrow-band imaging for a few high-z LAEs (Bond et al. 2010; Finkelstein et al. 2011), and they reached contradictory conclusions: Bond et al. (2010) suggested that Lyα sizes are compact and similar to UV continuum emission; but Finkelstein et al. (2011) posited that Lyα appears larger than the UV continuum.

Many ground-based studies of Lyα morphology suggest that a large-scale faint Lyα halo is common in high-z Lyα galaxies, due to the scatterings of Lyα photons by the H I gas in the circum-galactic medium (e.g., Møller & Warren 1998; Swinbank et al. 2007; Rauch et al. 2008; Steidel et al. 2011; Matsuda et al. 2012; Feldmeier et al. 2013 Momose et al. 2014; Wisotzki et al. 2016; Matthee et al. 2016). As the ground-based data has low spatial resolution, however, it is still unclear if the Lyα morphology of LAEs on galactic scales is compact or larger than the UV continuum, or if they show central Lyα absorption.

Green Pea galaxies are compact starburst galaxies with strong [O III]λ5007 emission lines (EW([O III]λ5007) > 300 Å) in the nearby universe (Cardamone et al. 2009). They have strong Lyα emission lines (Jaskot & Oey 2014; Henry et al. 2015; Yang et al. 2016) and their Lyα EW distribution is similar to high-z LAEs (Yang et al. 2016). Five Green Peas in our sample also show Lyman-continuum (LyC) emission (Izotov et al. 2016). In this paper, we study the spatial distribution of Lyα and UV emission of 24 Green Peas with *HST*-Cosmic Origins Spectrograph (COS), compare the spatial

Table 1
The Sample

ID (1)	R.A. (2)	Decl. (3)	Redshift (4)	EW(Lyα) Å (5)	$f_{\rm esc}^{\rm Ly\alpha}$ (6)	WP Å (7)	LP# (8)	GO# (9)
GP1333+6246[a]	13:33:03.94	+62:46:03.7	0.318124	65.3	1.066	1623	3	13744
GP1559+0841	15:59:25.98	+08:41:19.1	0.297036	89.0	0.682	1623	3	14201
GP1219+1526	12:19:03.98	+15:26:08.5	0.195599	157.5	0.672	1623	2	12928
GP1442−0209[a]	14:42:31.37	−02:09:52.8	0.293669	127.9	0.408	1623	3	13744
GP1503+3644[a]	15:03:42.82	+36:44:50.8	0.355689	99.6	0.402	1623	3	13744
GP1249+1234	12:48:34.64	+12:34:02.9	0.263389	94.8	0.384	1623	2	12928
GP1133+6514	11:33:03.80	+65:13:41.3	0.241397	35.3	0.352	1600	2	12928
GP1009+2916	10:09:18.99	+29:16:21.5	0.221918	62.5	0.335	1589	3	14201
GP1152+3400[a]	11:52:04.88	+34:00:49.9	0.341946	67.5	0.260	1623	3	13744
GP0926+4428	09:26:00.44	+44:27:36.5	0.180690	40.8	0.245	1611	1	11727
GP0925+1403[a]	09:25:32.37	+14:03:13.1	0.301211	83.0	0.171	1623	3	13744
GP0911+1831	09:11:13.34	+18:31:08.2	0.262200	49.5	0.155	1623	2	12928
GP0917+3152	09:17:02.52	+31:52:20.6	0.300364	31.0	0.138	1623	3	14201
GP1137+3524	11:37:22.14	+35:24:26.7	0.194390	33.4	0.130	1623	2	12928
GP1429+0643	14:29:47.03	+06:43:34.9	0.173509	35.7	0.103	1600	2	13017
GP1440+4619	14:40:09.94	+46:19:36.9	0.300758	26.8	0.101	1623	3	14201
GP1054+5238	10:53:30.83	+52:37:52.9	0.252638	10.7	0.068	1611	2	12928
GP1244+0216	12:44:23.37	+02:15:40.4	0.239426	40.0	0.065	1600	2	12928
GP0303−0759	03:03:21.41	−07:59:23.2	0.164880	7.2	0.050	1589	2	12928
GP1018+4106	10:18:03.24	+41:06:21.1	0.237052	26.1	0.047	1600	3	14201
GP1454+4528	14:54:35.58	+45:28:56.3	0.268505	23.0	0.047	1623	3	14201
GP2237+1336	22:37:35.06	+13:36:47.0	0.293501	9.9	0.034	1623	3	14201
GP0751+1638	07:51:57.80	+16:38:13.2	0.264713	8.8	0.024	1623	3	14201
GP1457+2232	14:57:35.13	+22:32:01.8	0.148611	5.3	0.010	1577	2	13293

Notes. Column descriptions: (5–6) restframe Lyα equivalent width, and Lyα escape fraction from Yang et al. (2017); (7) Central wavelength position of G160M grating; (8) COS lifetime position (LP); (9) *HST* programs: GO14201 (PI S. Malhotra), GO13744 (PI T. Thuan; Izotov et al. 2016), GO13293 (PI A. Jaskot; Jaskot & Oey 2014), GO12928 (PI A. Henry; Henry et al. 2015), GO11727 and GO13017 (PI T. Heckman; Heckman et al. 2011; Alexandroff et al. 2015).
[a] These are confirmed LyC leakers from Izotov et al. (2016).

profiles of Lyα photons at blue and red velocities, and discuss the implications to Lyα and LyC escape.

2. Observations and Data Analysis

In Yang et al. (2017), we assemble a sample of 43 Green Peas with *HST*-COS spectroscopic observations. Comparing to the parent sample of Green Peas in Cardamone et al. (2009), this sample covers the full ranges of properties, such as dust extinction, metallicity, and star-formation rate (Figure 1 in Yang et al. 2017). Thus, it is a representative sample of Green Peas. From this sample, we select 24 Green Peas that have good spatial resolution, i.e., full width at half maximum (FWHM) $\sim 0\farcs3$–$0\farcs4$ for the point source, in their 2D spectra. Because the COS FUV channel is not corrected for spherical aberration, the cross-dispersion resolution of COS FUV spectra depends on the chosen grating, the wavelength position (WP) of the grating, and the wavelength (COS ISR2013_07). The grating and WP are chosen based on considerations of wavelength coverages and the gap in FUV detectors, and thus vary mostly with the redshifts. Although this sample only covers a small redshift range (∼0.1–0.3), a slightly different redshift, and thus a different grating WP, can result in very different spatial resolution in the 2D spectra. Thus, these 24 selected Green Peas are not statistically different from the sample of 43 Green Peas, in obvious ways.

High-resolution NUV acquisition images were taken with the COS acquisition mode ACS/IMAGE for all 24 Green Peas. Their FUV spectra were taken with the $2\farcs5$-diameter Primary Science Aperture and the G160M grating, which has the best spatial resolution of the COS gratings.

The COS FUV grating G160M has five WP—1577, 1589, 1600, 1611, 1623 Å. The WP = 1623 Å has the best spatial resolution, and 15/24 of Green Peas are taken in this WP. The COS spatial resolutions are about $0.3 - 0\farcs4$ for point source and stable with wavelength for the WP = 1600, 1611, and 1623 Å, but are larger and vary moderately with wavelength for the WP = 1577 and 1589 Å. We generally avoid using objects with WP = 1577 Å or 1589 Å, except for three cases where their Lyα emission lines are in wavelength ranges with small spatial resolution. The WP of each object is shown in Table 1.

We retrieved COS spectra of these 24 Green Peas from the *HST* MAST archive after they had been processed through the standard COS pipeline. The calibrated two-dimensional Lyα and FUV spectra are shown in Figure 1. We extract the spatial profiles of Lyα along the sky direction by summing the spectra in a wavelength range about 1211−1220 Å, along the dispersion direction. We extract the spatial profiles of FUV continuum in wide wavelength ranges of a few tens of Angstroms, near Lyα lines in the same spectra segment. We then sum the spatial profiles from spectra taken at different central wavelengths or FP-POS settings for each Green Pea. In Figure 2, we show their normalized spatial profiles of Lyα and FUV continuum light. The pixel scale along the sky direction is $0\farcs1$/pixel. Because the COS FUV detector counts photons, we assume the photon counts in each spatial bin follows Poisson statistics, and calculate its statistical error as $\mathrm{counts_{err}} = (\mathrm{counts})^{1/2}$.

In Figure 2, we also show the instrumental spatial profile of each object, derived from observations of a point source in the

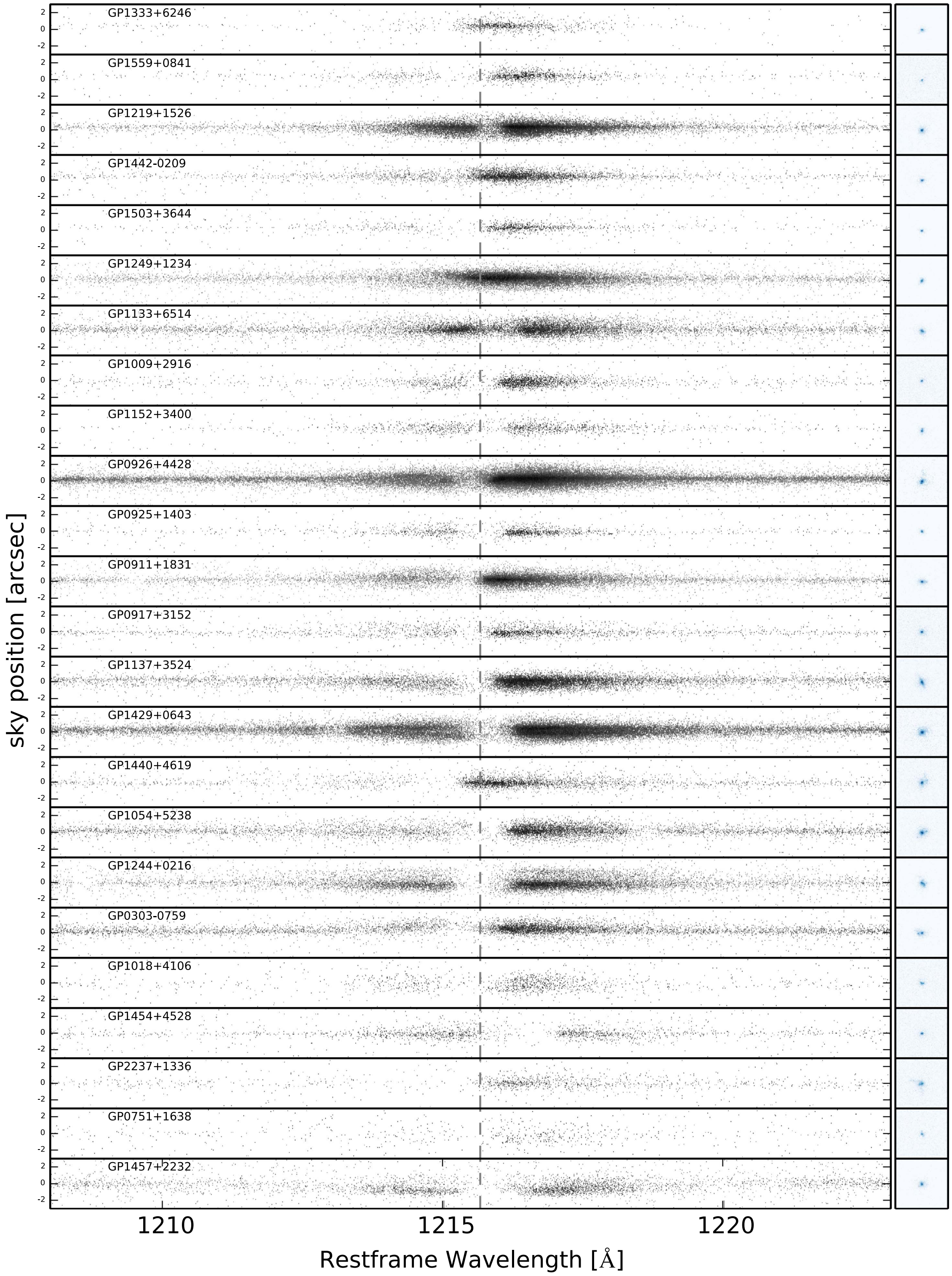

Figure 1. The 2D FUV spectra and NUV images of these 24 Green Peas. In the 2D spectra, the *x*-axis is along the dispersion direction and the *y*-axis is along the sky direction. The COS aperture is a circle with a diameter of 2.5 arcsec. The dashed vertical line marks the restframe wavelength of Lyα. The NUV images ($6'' \times 6''$) are at the same orientation as the 2D spectra. All NUV images have the same range of color-bar in log-scale. These 24 galaxies are sorted by decreasing $f_{\rm esc}^{\rm Ly\alpha}$ from top to bottom. The ID of each galaxy is marked in each panel.

same grating and WP (WD1057+719, CAL/COS 12806, PI: Derck Massa). Because the spatial resolution slightly varies with wavelength, the instrumental profiles are extracted separately for the Lyα and FUV continua in the corresponding wavelength ranges that are used to extract the Lyα and FUV spectra of each object.

The response of COS/FUV detector decreases with usage, a process called gain-sag. To mitigate these gain-sag effects, COS/FUV spectra are moved to pristine locations of the detector, i.e., different lifetime positions (LP), every 2–3 years. Our sample spans all three LPs (LP1, LP2, and LP3). As we only use the data with small spatial resolution, the spatial

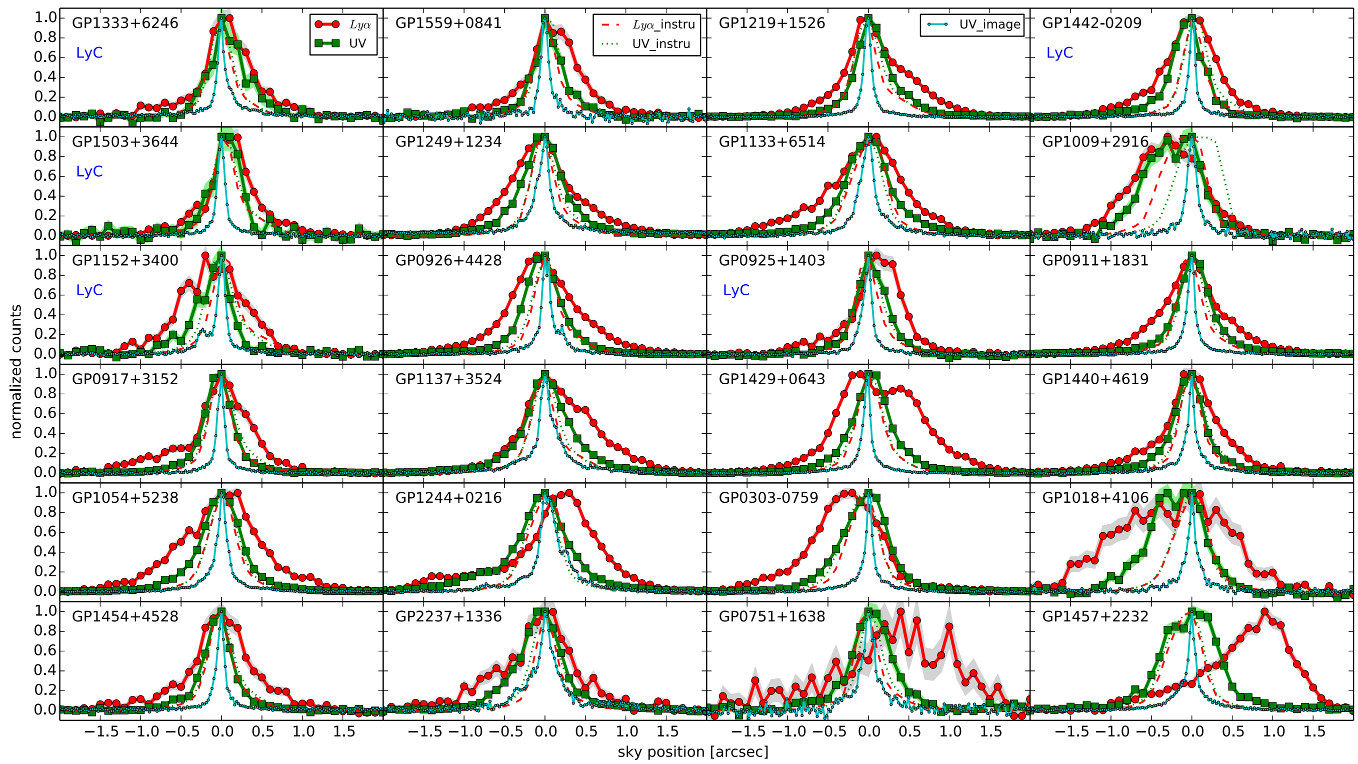

Figure 2. The normalized spatial profiles along the sky direction for the 24 Green Peas. In each panel, the solid green line with a square marker shows the spatial profiles of the UV continuum emission measured from COS, and the solid red line with circle marker shows the spatial profiles of total Lyα emission. The shaded gray (light-green) regions of the solid red (green) lines show the 1σ errors of the Lyα (UV) spatial profiles. The dotted green and dashed red lines show the instrumental spatial profiles for UV continuum and Lyα emission, respectively. The instrumental spatial profiles are derived from observations of a white dwarf point source (Section 2). The solid cyan line with dot marker shows the spatial profiles of UV continuum emission, measured from the NUV acquisition image along the spatial direction of 2D spectra. These 24 galaxies are sorted by decreasing $f_{\rm esc}^{\rm Ly\alpha}$ from top to bottom and left to right. Five LyC leakers in this sample (Izotov et al. 2016) are marked with "LyC."

profiles are separated from the insensitive detector regions of earlier LPs. The LP of each object is shown in Table 1.

We then measure the Lyα EW and Lyα escape fraction ($f_{\rm esc}^{\rm Ly\alpha}$) of this sample (details in Yang et al. 2017). The $f_{\rm esc}^{\rm Ly\alpha}$ is defined as the ratio of the measured Lyα flux to intrinsic Lyα flux. Assuming case-B recombination, the intrinsic Lyα flux is about 8.7 times the dust-extinction-corrected Hα flux measured from SDSS spectra. Thus, the $f_{\rm esc}^{\rm Ly\alpha}$ is Lyα(observed)/(8.7 $\times$ H$\alpha_{\rm corrected}$). In Table 1, we show their redshifts, Lyα EWs, and Lyα escape fractions.

3. Compare Spatial Profiles of Lyα and UV emission

From the 2D spectra and 1D spatial profiles, we can see that the Lyα emission comes from a larger region than the FUV emission in most of these 24 Green Peas. The spatial profiles of UV are only slightly larger than the instrumental profiles, but the spatial profiles of Lyα are well-resolved and show asymmetric spatial distributions in many cases. In four cases with low $f_{\rm esc}^{\rm Ly\alpha}$ (GP1457+2232, GP0303−0759, GP0752+1638, and GP1244+0216), Lyα light shows a significant offset from the FUV continuum (similar to some high-z LAEs in Micheva et al. 2015). In GP1429+0643, a large fraction of the Lyα emission in the galactic center is absorbed, resulting in a double-horned spatial profile.

To characterize the size of spatial profile, we measure the FWHM (FWHM$_m$) of each profile. The FWHM is not sensitive to the depth of the observation. To get the error of FWHM$_m$ for each observed spatial profile, we simulate 1000 fake profiles by adding random Gaussian errors to the observed profile. We measure the FWHM$_m$ of each fake profile and calculate the standard deviation of the 1000 fake profiles as the error of FWHM$_m$ for each observed spatial profile. The measured FWHM$_m$ and its errors are shown in Table 2. We can see again that the Lyα emission have significantly larger FWHM$_m$ than the UV continuum emission.

3.1. The Deconvolved Sizes of Lyα and UV Emission

To estimate the deconvolved sizes, we assume that the intrinsic Lyα or UV emission follows an exponential profile with scale radius r_e, and convolve the exponential profile with the instrumental profile, so we get a relation between observed FWHM and intrinsic FWHM. Because the throughput begins to decrease when the offset from aperture center is larger than about 0$''$.5, we multiply the convolved profile with a throughput curve of G160M, retrieved from COS instrumental handbook. In Figure 3, we show an example of the profile convolution and how the FWHM of convolved profile varies with the r_e of intrinsic profile. We then calculate the deconvolved size of Lyα emission as the FWHM of the exponential profile that has the same FWHM$_m$ as the observed Lyα spatial profile. Because the measured FWHM$_m$ of Lyα emission (about 0$''$.6–1$''$.0) are within the angular ranges with $\gtrsim$80% throughput, the Lyα sizes are *not* underestimated due to attenuation at large offsets, except in GP1018+4106, which has very large Lyα size.

Because the NUV image has a spatial resolution of about 0$''$.04 (less than two pixels, at a scale of 0$''$.0235/pixel), the NUV emissions of this sample are well-resolved. We estimate the NUV size from the NUV acquisition image shown in

Table 2
Measurements of Lyα and UV Sizes

ID (1)	FWHM$_m$(Lyα) arcsec (2)	FWHM$_m$(FUV) arcsec (3)	FWHM$_d$(Lyα) arcsec (4)	FWHM$_d$(FUV) arcsec (5)	FWHM(NUV) arcsec (6)	$\frac{\text{FWHM(Ly}\alpha)}{\text{FWHM(UV)}}$ (7)
GP1333+6246[a]	0.56 ± 0.04	0.38 ± 0.08	$0.24^{+0.04}_{-0.03}$	$0.08^{+0.07}_{-0.07}$	0.09	$2.62^{+0.80}_{-0.52}$
GP1559+0841	0.56 ± 0.04	0.35 ± 0.04	$0.25^{+0.04}_{-0.04}$	$0.04^{+0.04}_{-0.03}$	0.11	$2.27^{+0.67}_{-0.55}$
GP1219+1526	0.65 ± 0.03	0.42 ± 0.01	$0.29^{+0.01}_{-0.03}$	$0.06^{+0.01}_{-0.01}$	0.11	$2.65^{+0.43}_{-0.47}$
GP1442−0209[a]	0.70 ± 0.04	0.44 ± 0.03	$0.37^{+0.04}_{-0.04}$	$0.12^{+0.03}_{-0.03}$	0.08	$3.00^{+1.29}_{-0.82}$
GP1503+3644[a]	0.48 ± 0.04	0.38 ± 0.06	$0.15^{+0.03}_{-0.03}$	$0.06^{+0.06}_{-0.04}$	0.11	$1.39^{+0.43}_{-0.36}$
GP1249+1234	0.75 ± 0.02	0.56 ± 0.02	$0.39^{+0.03}_{-0.01}$	$0.19^{+0.01}_{-0.01}$	0.17	$2.00^{+0.31}_{-0.20}$
GP1133+6514	0.96 ± 0.06	0.58 ± 0.01	$0.54^{+0.07}_{-0.07}$	$0.17^{+0.01}_{-0.01}$	0.20	$2.70^{+0.69}_{-0.56}$
GP1009+2916	0.95 ± 0.06	0.82 ± 0.04	$0.46^{+0.07}_{-0.07}$	$0.30^{+0.06}_{-0.06}$	0.14	$1.50^{+0.61}_{-0.42}$
GP1152+3400[a]	0.87 ± 0.09	0.44 ± 0.07	$0.47^{+0.08}_{-0.10}$	$0.08^{+0.06}_{-0.07}$	0.11	$4.28^{+1.32}_{-1.19}$
GP0926+4428	0.82 ± 0.01	0.49 ± 0.01	$0.44^{+0.01}_{-0.01}$	$0.14^{+0.01}_{-0.01}$	0.12	$3.20^{+0.47}_{-0.38}$
GP0925+1403[a]	0.58 ± 0.04	0.42 ± 0.03	$0.26^{+0.03}_{-0.03}$	$0.08^{+0.01}_{-0.03}$	0.12	$2.19^{+0.50}_{-0.41}$
GP0911+1831	0.62 ± 0.02	0.44 ± 0.01	$0.28^{+0.03}_{-0.01}$	$0.11^{+0.01}_{-0.01}$	0.10	$2.50^{+0.64}_{-0.39}$
GP0917+3152	0.62 ± 0.04	0.39 ± 0.01	$0.30^{+0.04}_{-0.04}$	$0.04^{+0.01}_{-0.03}$	0.10	$3.05^{+0.80}_{-0.66}$
GP1137+3524	0.88 ± 0.02	0.56 ± 0.01	$0.49^{+0.03}_{-0.01}$	$0.19^{+0.01}_{-0.01}$	0.18	$2.50^{+0.35}_{-0.23}$
GP1429+0643	1.18 ± 0.02	0.49 ± 0.01	$0.90^{+0.01}_{-0.07}$	$0.12^{+0.01}_{-0.01}$	0.09	$7.22^{+1.03}_{-1.22}$
GP1440+4619	0.62 ± 0.04	0.42 ± 0.01	$0.29^{+0.04}_{-0.03}$	$0.07^{+0.01}_{-0.01}$	0.08	$3.64^{+0.98}_{-0.65}$
GP1054+5238	0.99 ± 0.07	0.54 ± 0.01	$0.62^{+0.10}_{-0.08}$	$0.17^{+0.01}_{-0.01}$	0.13	$3.75^{+0.98}_{-0.75}$
GP1244+0216	0.82 ± 0.03	0.63 ± 0.02	$0.39^{+0.04}_{-0.03}$	$0.22^{+0.01}_{-0.03}$	0.24	$1.62^{+0.37}_{-0.25}$
GP0303−0759	0.94 ± 0.04	0.63 ± 0.02	$0.55^{+0.04}_{-0.04}$	$0.19^{+0.01}_{-0.01}$	0.08	$2.86^{+0.45}_{-0.39}$
GP1018+4106	1.75 ± 0.27	0.76 ± 0.04	$2.15^{+1.80}_{-0.83}$	$0.33^{+0.04}_{-0.03}$	0.10	$6.46^{+6.50}_{-2.94}$
GP1454+4528	0.62 ± 0.05	0.37 ± 0.02	$0.29^{+0.04}_{-0.06}$	$0.01^{+0.04}_{-0.01}$	0.10	$2.91^{+0.79}_{-0.77}$
GP2237+1336	0.68 ± 0.11	0.56 ± 0.03	$0.36^{+0.10}_{-0.11}$	$0.18^{+0.03}_{-0.01}$	0.20	$1.80^{+0.74}_{-0.67}$
GP0751+1638	0.97 ± 0.32	0.53 ± 0.04	$0.62^{+0.42}_{-0.32}$	$0.19^{+0.04}_{-0.03}$	0.17	$3.21^{+3.04}_{-1.92}$
GP1457+2232	0.92 ± 0.09	0.80 ± 0.03	$0.50^{+0.10}_{-0.10}$	$0.33^{+0.04}_{-0.03}$	0.10	$1.50^{+0.45}_{-0.43}$

Notes. Column descriptions: (2–3) measured FWHM of Lyα and UV spatial profiles. (4–5) FWHM$_d$(Lyα) and FWHM$_d$(FUV) are deconvolved FWHM of Lyα and UV derived by mapping measured FWHM to intrinsic values (see Section 3.1 and Figure 3). (6) FWHM of 1D NUV profile. We convert the 2D NUV images into a 1D profile along the sky direction of spectra. (7) Ratios of FWHM(Lyα) to FWHM(UV). When calculating the ratio, we use the larger one of FWHM$_d$(FUV) and FWHM(NUV). These 24 galaxies are sorted by decreasing $f_{\rm esc}^{\rm Ly\alpha}$ from top to bottom.
[a] These are confirmed LyC leakers from Izotov et al. (2016).

Figure 1 at the same orientation as the 2D spectra. We extract spatial profiles by summing the pixels in the image along the dispersion direction. We then calculate the intrinsic NUV sizes as the FWHM of the NUV spatial profiles. The results are shown in Table 2.

Ideally, the deconvolved FUV size and NUV size should be similar. However, when the observed FUV profile and instrumental profile are very similar, the deconvolution failed and resulted in very small deconvolved FUV size. To compare the sizes of Lyα and UV emission, we use the larger of FWHM$_d$(FUV) or FWHM(NUV), so we get a conservative Lyα-to-UV size ratio. The deconvolved Lyα sizes are typically 2.6 times larger than the UV sizes, and vary between 1.4 and 4.3 times the size for 22 out of the 24 Green Peas. In GP1429+0643, which has a double-horned spatial profile, the deconvolved Lyα FWHM is about seven times the UV FWHM. In GP1018+4106, the deconvolved Lyα FWHM is badly constrained and can be 3.5–13 times larger than the UV FWHM.

4. Comparing Spatial Profiles of Lyα Photons at Different Velocities

Green Peas usually show double-peaked Lyα velocity profiles (Jaskot & Oey 2014; Henry et al. 2015; Yang et al. 2016). The Lyα photons with different velocities are scattered differently by the H I gas. Because we have the 2D Lyα spectra, we can compare the spatial profiles of Lyα photons at different velocities. We define the blue-part (red-part) as the negative-velocity-side (positive-velocity-side) of the inter-peak dip of the Lyα velocity profile. For one object (GP1249+1234) with a single-peaked Lyα velocity profile, we separate the blue and red parts by velocity = 0. We then extract the spatial profiles of the blue- and red-part Lyα emissions. Because the blue is usually weaker than the red-part Lyα emission, we show the 8 of 24 Green Peas with the best signal-to-noise ratio in the blue-part Lyα emission. These eight Green Peas also have relatively high $f_{\rm esc}^{\rm Ly\alpha}$. We compare their spatial profiles of blue-part and red-part Lyα emissions in Figure 4.

The spatial profiles of blue-part and red-part Lyα emissions are generally similar. However, in four cases (GP1137+3524, GP1249+1234, GP0911+1831, and GP0926+4428), the blue-part Lyα emissions are more extended than the red-part Lyα emissions. In the other four cases (GP1244+0216, GP1133+6514, GP1429+0643, and GP1219+1526), the blue-part and red-part Lyα emissions are very similar. We also noticed that the Lyα spatial profiles show a relation with the Lyα velocity profiles—the objects with weaker blue peaks in the Lyα velocity profile (i.e., small flux ratio of blue-part to red-part Lyα emission), such as GP1137+3524, GP0911+1831, and GP0926+4428, also have broader blue-part spatial profiles. On

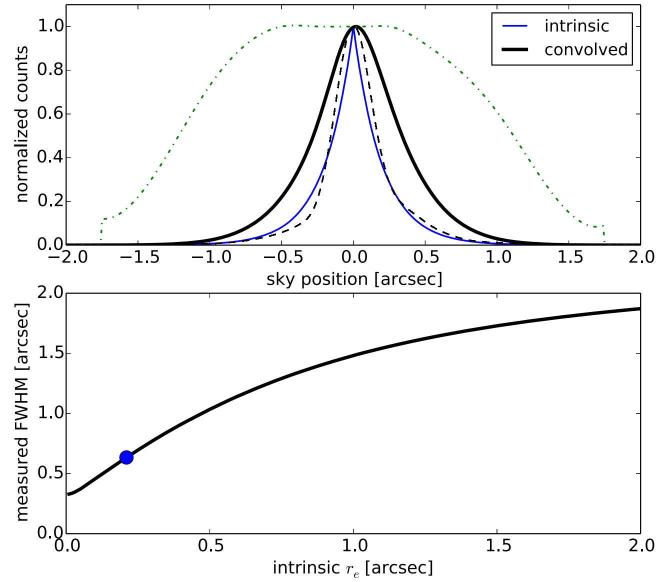

Figure 3. Top panel: an example of the profile convolution. The dashed black line is a typical instrumental profile for Lyα emission. The thin solid blue line shows the intrinsic spatial profile of Lyα emission, which is assumed to be an exponential profile (a typical profile with $r_e = 0\farcs2$ is shown). The thick solid black line is the convolved profile after convolving the intrinsic profile with the instrumental profile and multiplying it by the throughput profile (dashed–dotted green line). Bottom panel: the measured FWHM of the convolved profile as a function of the r_e of the intrinsic profile. The blue point shows a typical value of the intrinsic Lyα size in our sample.

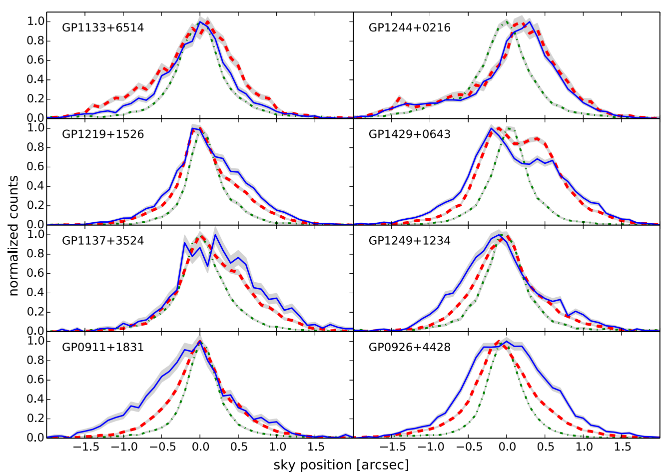

Figure 4. Comparison between the spatial profiles of the blueshifted and redshifted portions of the Lyα emission lines for eight objects with the best signal-to-noise ratio in the blue-part Lyα emission. Because the Lyα velocity profiles are usually double-peaked, we define the blue-part (red-part) as the negative-velocity-side (positive-velocity-side) of the inter-peak dip of the Lyα velocity profile. The solid blue lines, dashed red lines, and dotted green lines show the spatial profiles of blue-part Lyα, red-part Lyα, and UV continuum emission, respectively. The shaded gray regions of lines show the 1σ errors of the spatial profiles.

the other hand, GP1133+6514, which has the strongest blue peak in its Lyα velocity profile, seems to show slightly more compact blue-part than red-part Lyα emission.

In four Green Peas (GP1219+1526, GP1133+6514, GP0926+4428, and GP1429+0643), the Lyα velocity profiles show large residual emission at velocities near zero. From their 2D spectra (Figure 1), we find that the Lyα emission at a velocity near zero seems to have more extended Lyα emission than the Lyα emission at other velocities.

Because the outflowing H I gas presented in many Green Peas has larger optical depth for the blue-part Lyα photons than the red-part Lyα photons, we expect that the escaped blue-part Lyα photons went through more scatterings on average, and were scattered to larger radius. For the Lyα photons at velocities near zero, the optical depth is the largest and their spatial profiles also show the largest sizes.

5. Discussion

5.1. Comparison to Previous Results

Many studies have measured the Lyα morphology of some nearby star-forming galaxies with *HST*/STIS (Mas-Hesse et al. 2003) and *HST*/ACS images (e.g., Kunth et al. 2003; Hayes et al. 2005; Östlin et al. 2009, 2014). Mas-Hesse et al. (2003) analyzed the *HST*/STIS 2D spectra of Lyα and UV emission and showed that both Haro 2 and IRAS 0833+6517 have low Lyα EW (6 and 12 Å) and larger Lyα sizes than UV continuum sizes, and that their Lyα peaks are offset from the peaks of UV continuum emission.

The LARS program studies the Lyα morphology of 14 nearby starburst galaxies (Hayes et al. 2014; Östlin et al. 2014). Nine out of the 14 galaxies have low Lyα EW and escape fraction. They also show Lyα absorption or weak Lyα emission in the central part of galaxy, and diffuse Lyα emission in the outer part of the galaxy. The other five galaxies (LARS01, 02, 05, 07, and 14; LARS14 is galaxy GP0926+4428 in our sample) are LAEs with relatively high Lyα EW and comparable to most of the Green Peas in our sample. These five galaxies also have [O III]λ5007 equivalent widths around 200−300 Å in their SDSS spectra. The Lyα emission in LARS01 shows an offset from the UV emission, and is very similar to the four cases with Lyα-UV offsets in our sample. The Lyα emission in LARS05 shows partial central absorption and is very similar to GP1429+0643, the double-horned case in our sample. The 20% Petrosian radii of the Lyα emissions of these five galaxies are 2.3–3.6 times larger than the 20% Petrosian radii of Hα emission (Hayes et al. 2014), which makes them very similar to the Lyα/UV FWHM ratios in our sample.

Two studies measure Lyα sizes of five high-z LAEs with high-resolution *HST* narrow-band imaging (Bond et al. 2010; Finkelstein et al. 2011). Bond et al. (2010) suggested that Lyα sizes are compact and similar to UV emission, but Finkelstein et al. (2011) posited that the half light radius of Lyα appears ~1.6 times larger than the half light radius of UV continuum. These narrow-band *HST* images of high-z LAEs are very hard to obtain and have low S/Ns. Thus, the Lyα and UV sizes of low-z LAEs are valuable. Because Green Peas are analogs of high-z LAEs, our results suggest that most high-z LAEs likely have larger Lyα than UV sizes. The extended Lyα emission probably indicates gas outflows around galaxies illuminated by Lyα light.

One interesting question regards the redshift evolution of Lyα sizes of LAEs. Recently, Wisotzki et al. (2016) measured Lyα radial profiles of a sample of LAEs at $z = 3$–6 from VLT/MUSE data. They found that, in 12 LAEs with both Lyα and UV continuum sizes, the Lyα light is considerably more extended than the UV continuum light. Here, we compare the sizes of Green Peas and the MUSE LAEs. Using the Lyα radial profiles in Wisotzki et al. (2016), we measured the deconvolved Lyα scale radius r_e, assuming intrinsic exponential

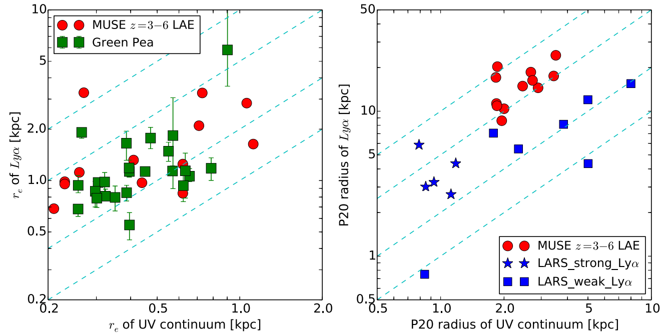

Figure 5. Left: Comparison of the Lyα-to-UV scale length of Green Peas (green squares) and MUSE $z = 3$–6 LAEs sample (red dots) (Wisotzki et al. 2016). The Lyα scale lengths of MUSE LAEs are measured from the radial profile in Wisotzki et al. (2016) using the same method as Green Peas. Right: Comparison of the Lyα-to-UV Petrosian 20% (P20) radius of LARS ~ 0 galaxies and MUSE LAEs. Notice that the Petrosian 20% radius of MUSE sample is measured from the best-fit model of radial profile. The dashed cyan lines show constant ratios of 1:1, 2:1, 5:1, and 10:1.

profiles, so that the methods are same when measuring the r_e of MUSE LAES and Green Peas. As shown in Figure 5, the Lyα-to-UV size ratios of Green Peas and MUSE LAEs are very similar. Notice that some MUSE LAEs have extended Lyα halos far beyond the scale radius. For Green Peas, however, we do not have robust data to characterize the Lyα emission beyond a few Kpcs.

In the right panel of Figure 5, we compare the Petrosian 20% radius (R_{P20}) of MUSE LAEs (Table 2 in Wisotzki et al. (2016)) to that of the LARS sample (Table 1 in Hayes et al. 2014). Compared to the five strong Lyα emitters in LARS sample (marked by stars, LARS01, 02, 05, 07, and 14), the MUSE LAEs only have about two times larger ratios of R_{P20}(Lyα) to R_{P20}(UV). One caveat of the comparison is that the Petrosian radius of MUSE sample is measured from the best-fit *model* of radial profile, instead of the observed data, which is different from the method used in the LARS sample. This might be the reason that the R_{P20}(UV) of MUSE LAEs are about 2–4 kpc, approximately a factor of three larger than the R_{P20}(UV) of the five LARS Lyα emitters.

Based on our rough comparison of Green Peas and MUSE LAEs, the scale lengths of Lyα and UV continuum have small evolution with redshift. This is not surprising, considering that Green Peas and high-z LAEs have very similar galactic properties, such as stellar mass, star formation rate, and starburst age. The starburst in Green Peas and LAEs can drive gas outflows to the outer part of galaxies, and the gas outflows can scatter the Lyα light and cause the extended Lyα emission.

5.2. Implication for Lyα and LyC Escape

Our results indicate that Lyα have larger sizes than the UV continuum. Because Lyα is a resonant line, our results suggest that most Lyα photons escape out of a galaxy through many resonant scatterings in the low H I column density gas in Green Peas. If there are fewer scatterings in the Lyα escape process, the Lyα escape fraction would be higher and the Lyα emission would be more compact. Thus, there may be an anti-correlation between $f_{\mathrm{esc}}^{\mathrm{Ly}\alpha}$ and the size of Lyα light. In Figure 6, we show the relation between $f_{\mathrm{esc}}^{\mathrm{Ly}\alpha}$ and the size ratio of FWHM(Lyα)/FWHM(UV) (column (7) of Table 2). The scatter is large, but it shows a weak trend for objects with $f_{\mathrm{esc}}^{\mathrm{Ly}\alpha} \gtrsim 0.1$, indicating that LAEs with higher $f_{\mathrm{esc}}^{\mathrm{Ly}\alpha}$ have *more compact* Lyα morphology.

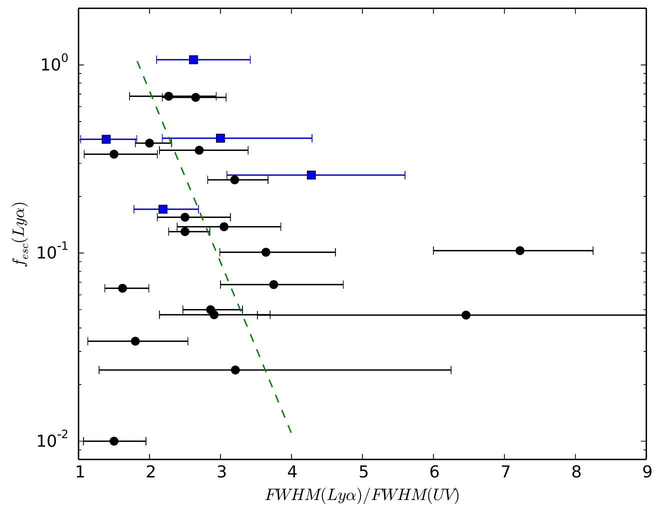

Figure 6. The relation between $f_{\mathrm{esc}}^{\mathrm{Ly}\alpha}$ and the size ratio of FWHM(Lyα)/FWHM(UV) (column (7) of Table 2). The blue square shows the five LyC leakers in this sample. The dashed green line shows a linear fit to the points with $f_{\mathrm{esc}}^{\mathrm{Ly}\alpha} > 0.1$. The Spearman correlation coefficient for the points with with $f_{\mathrm{esc}}^{\mathrm{Ly}\alpha} > 0.1$ is $r = -0.41$ with null probability = 0.11.

In Figure 6, we also mark the five LyC leakers with blue squares. These LyC leakers have Lyα-to-UV continuum size ratios similar to the other Green Peas. We note that the other Green Peas could be unknown LyC leakers, as their current UV spectra ranges do not cover the LyC emission. The LyC leakers have 1.4–4.3 times larger Lyα sizes than the UV continuum sizes, so most H I gas, which scatters Lyα emission, is unlikely to be transparent to the LyC emission. Therefore, the LyC emission of these LyC leakers probably escape through ionized holes in the interstellar medium.

6. Conclusion

We have investigated the Lyα and UV sizes of Green Pea galaxies using their *HST*-COS 2D spectra. Our main results are as follows.

1. We compared Lyα and UV sizes from the 2D spectra and 1D spatial profiles, and found that most Green Peas show more extended Lyα emission than the UV continuum. We also measured the deconvolved FWHM of the spatial profiles as their Lyα and UV sizes. The Lyα sizes in most Green Peas of this sample are about 2–4 times larger than their UV continuum sizes. We also found that the five LyC leakers in our sample have larger Lyα than UV continuum sizes by 1.4–4.3 times.
2. In eight Green Peas, we compared the spatial profiles of Lyα photons at blueshifted and redshifted velocities, and found the blue wing of the Lyα line has a larger spatial extent than the red wing in four Green Peas with comparatively weak blue Lyα line wings.
3. Because Green Peas are analogs of high-z LAEs, our results suggest that most high-z LAEs likely have larger Lyα than UV sizes. We also show that Green Peas and the MUSE $z = 3$–6 LAEs sample have similar Lyα-to-UV continuum size ratios.
4. We compared the Lyα escape fraction with the size ratio FWHM(Lyα)/FWHM(UV), and found that, for those Green Peas with $f_{\mathrm{esc}}^{\mathrm{Ly}\alpha} > 10\%$, objects with higher $f_{\mathrm{esc}}^{\mathrm{Ly}\alpha}$ tend to have *more compact* Lyα morphology.

These imaging and spectroscopy data are based on observations with the NASA / ESA *Hubble Space Telescope*, (GO11727, GO12928, GO13293, GO13017, GO13744, GO14201), obtained at the Space Telescope Science Institute, which is operated by the Association of Universities for Research in Astronomy (AURA), Inc., under NASA contract NAS 5-26555. Some of the data presented in this paper were obtained from the Mikulski Archive for Space Telescopes (MAST). STScI is operated by the Association of Universities for Research in Astronomy, Inc., under NASA contract NAS5-26555. Support for MAST for non-*HST* data is provided by the NASA Office of Space Science via grant NNX09AF08G, and by other grants and contracts. H.Y. acknowledges support from China Scholarship Council. H.Y. and J.X.W. are grateful for support from NSFC 11421303, CAS Frontier Science Key Research Program (QYZDJ-SSW-SLH006), and the Strategic Priority Research Program "The Emergence of Cosmological Structures" of the Chinese Academy of Sciences (grant No. XDB09000000). Partial support for this work was provided by NSF grant AST-1518057.

References

Alexandroff, R. M., Heckman, T. M., Borthakur, S., Overzier, R., & Leitherer, C. 2015, ApJ, 810, 104
Bond, N. A., Feldmeier, J. J., Matković, A., et al. 2010, ApJL, 716, L200
Cardamone, C., Schawinski, K., Sarzi, M., et al. 2009, MNRAS, 399, 1191
Charlot, S., & Fall, S. M. 1993, ApJ, 415, 580
Dey, A., Spinrad, H., Stern, D., Graham, J. R., & Chaffee, F. H. 1998, ApJL, 498, L93
Dijkstra, M., Haiman, Z., & Spaans, M. 2006, ApJ, 649, 14
Feldmeier, J. J., Hagen, A., Ciardullo, R., et al. 2013, ApJ, 776, 75
Finkelstein, S. L., Cohen, S. H., Windhorst, R. A., et al. 2011, ApJ, 735, 5
Hayes, M., Östlin, G., Duval, F., et al. 2014, ApJ, 782, 6
Hayes, M., Östlin, G., Mas-Hesse, J. M., et al. 2005, A&A, 438, 71
Heckman, T. M., Borthakur, S., Overzier, R., et al. 2011, ApJ, 730, 5
Henry, A., Scarlata, C., Martin, C. L., & Erb, D. 2015, ApJ, 809, 19
Hu, E. M., Cowie, L. L., & McMahon, R. G. 1998, ApJL, 502, L99
Izotov, Y. I., Schaerer, D., Thuan, T. X., et al. 2016, MNRAS, 461, 3683
Jaskot, A. E., & Oey, M. S. 2014, ApJ, 791, 19L
Kashikawa, N., Shimasaku, K., Matsuda, Y., et al. 2011, ApJ, 734, 119
Kunth, D., Leitherer, C., Mas-Hesse, J. M., Östlin, G., & Petrosian, A. 2003, ApJ, 597, 263
Malhotra, S., & Rhoads, J. E. 2004, ApJL, 617, L5
Mas-Hesse, J. M., Kunth, D., Tenorio-Tagle, G., et al. 2003, ApJ, 598, 858
Matsuda, Y., Yamada, T., Hayashino, T., et al. 2012, MNRAS, 425, 878
Matthee, J., Sobral, D., Oteo, I., et al. 2016, MNRAS, 458, 449
Matthee, J. J. A., Sobral, D., Swinbank, A. M., et al. 2014, MNRAS, 440, 2375
Micheva, G., Iwata, I., Inoue, A. K., et al. 2015, arXiv:1509.03996
Møller, P., & Warren, S. J. 1998, MNRAS, 299, 661
Momose, R., Ouchi, M., Nakajima, K., et al. 2014, MNRAS, 442, 110
Neufeld, D. A. 1990, ApJ, 350, 216
Östlin, G., Hayes, M., Duval, F., et al. 2014, ApJ, 797, 11
Östlin, G., Hayes, M., Kunth, D., et al. 2009, AJ, 138, 923
Ouchi, M., Shimasaku, K., Furusawa, H., et al. 2003, ApJ, 582, 60
Pentericci, L., Vanzella, E., Fontana, A., et al. 2014, ApJ, 793, 113
Rauch, M., Haehnelt, M., Bunker, A., et al. 2008, ApJ, 681, 856
Rhoads, J. E., Malhotra, S., Dey, A., et al. 2000, ApJL, 545, L85
Steidel, C. C., Bogosavljević, M., Shapley, A. E., et al. 2011, ApJ, 736, 160
Swinbank, A. M., Bower, R. G., Smith, G. P., et al. 2007, MNRAS, 376, 479
Tilvi, V., Papovich, C., Finkelstein, S. L., et al. 2014, ApJ, 794, 5
Treu, T., Trenti, M., Stiavelli, M., Auger, M. W., & Bradley, L. D. 2012, ApJ, 747, 27
Verhamme, A., Schaerer, D., & Maselli, A. 2006, A&A, 460, 397
Wisotzki, L., Bacon, R., Blaizot, J., et al. 2016, A&A, 587, A98
Yang, H., Malhotra, S., Gronke, M., et al. 2016, ApJ, 820, 130
Yang, H., Malhotra, S., Gronke, M., et al. 2017, arXiv:1701.01857
Zheng, Z., Cen, R., Trac, H., & Miralda-Escudé, J. 2010, ApJ, 716, 574
Zheng, Z.-Y., Malhotra, S., Rhoads, J. E., et al. 2016, ApJS, 226, 23